



Politecnico  
di Bari

Repository Istituzionale dei Prodotti della Ricerca del Politecnico di Bari

A Quantitative and Computer-Aided Thermography-Based Diagnostics for PV Devices—Part II: Platform and Results

This is a post print of the following article

*Original Citation:*

A Quantitative and Computer-Aided Thermography-Based Diagnostics for PV Devices—Part II: Platform and Results / Vergura, S., Colaprico, M., de Ruvo, M.F., Marino, F.. - In: IEEE JOURNAL OF PHOTOVOLTAICS. - ISSN 2156-3381. - 7:1(2017), pp. 237-243. [10.1109/JPHOTOV.2016.2614860]

*Availability:*

This version is available at <http://hdl.handle.net/11589/91481> since: 2022-06-08

*Published version*

DOI:10.1109/JPHOTOV.2016.2614860

Publisher:

*Terms of use:*

(Article begins on next page)

# A Quantitative and Computer Aided Thermography-based Diagnostics for PV Devices: Part II – Platform and Results

S. Vergura, *Senior Member, IEEE*, M. Colaprico, M. F. de Ruvo and F. Marino

**Abstract** — This paper *Part II* deals with the software platform that implements the workflow described in *Part I*, i.e. a thermography-based diagnostics able to provide a detailed, clear and unambiguous information on the health state of PV modules. The methodology, in fact, allows a numerical and qualitative evaluation of each cell of the PV module.

In particular, this paper deeply describes the main features of the software platform and introduces the Graphical User Interface that makes the framework efficiently and effectively adoptable, since it leads to the automatic generation of a report. In order to show the manifold features, three cases of study, deriving from a real monitoring survey are discussed, highlighting the critical situations revealed neither with a direct observation of the infrared image, nor with its manual processing: the first case regards a defected PV module, the second one an almost completely uniform module, while the third one deals with a dis-homogeneous module.

**Index Terms** — Thermography, computer aided diagnostics, digital image processing, PV cells, PV modules, PV devices, filtering.

## I. INTRODUCTION

Sometimes, the power losses in PhotoVoltaic (PV) modules are due either to the dust or to the dirt, but they also may depend on internal problems of the cells.

In order to monitor the performance of the PV systems, a lot of commercial software solutions have been proposed in the last years, since the diffusion of the PV technology speeded up. In this context, we prefer not naming some specific products rather than others, because anyone can have an idea about the many available solutions simply through a search on the Internet. Anyway, the most known software platforms have been generally conceived for the supervision of PV plants, and operate monitoring the values of electrical parameters, combined with the environmental ones.

Moreover, the depth of their probing is also related to the configuration of the PV system, and needs to take into account the presence of distributed or centralized inverters, the connection in parallel or not of the panels, and so on: in any case, this electrical monitoring never regards the single cells of a PV

module, because its grain is constituted by the entire PV module. Therefore, when problems arise at the cell level, advanced solutions have to be studied for whoever is interested in investigating the reasons of the power loss, and not simply its amount.

At the cell level, the above problems are classified as *defects*, which are essentially grouped in two main typologies [1]-[2]: *material-induced*, depending on the internal material structure, and *process-induced*, generated during the productive process. In order to deeper investigate these phenomena, some specific and known defects have been modelled and inserted in well-operating PV cells, and their thermal effects have been analyzed in [3], whereas models of PV cell, able to take into account the variable environmental conditions, are proposed in [4]-[5].

Anyway, it results that any defect manifests itself as over temperature, as reported in Table 3 of [6]. This effect makes the thermography a powerful tool for diagnostic purpose of PV modules [7], also compared or combined with other modern diagnostic techniques [8-10]. For instance, in [11] the thermographic analysis is used to identify the mismatch faults of PV modules; in [12] it is used for detecting snail trails and cell micro-cracks, and in [13] the thermography is proposed for improving the energy efficiency under partial shading conditions. Nevertheless, a PV module is constituted of many PV cells, but neither the simple thermography, nor the tools generally embedded into the thermo-cameras, nor image processors running on a PC, provide detailed information about each cell, since these *on-the-shelf* tools allow extrapolating only simple data (e.g. temperature of a selected pixel, mean of rectangular regions, histograms, etc.). For this aim, in the Part I [14], we have proposed a diagnostic workflow for carrying out an accurate analysis of each single PV cell, based on the automatic processing of the infrared image of the PV modules. Since the workflow encompasses several steps and many calculations, and the number of PV modules which is usually investigated during a maintenance campaign might be huge (e.g., 1-MWp PV plant can contain over 5,000 PV modules), in this Part II we present a software platform that, exploiting the OpenCV software library [15], implements the workflow and allows to perform a correct and fine diagnostics in a very short time. The platform is characterized by an easy-to-use Graphical User Interface (GUI) which follows step by step the workflow, making the partial results available to the user as soon as they are produced, so helping him in tuning the required diagnostic parameters. The results are displayed both in

---

S. Vergura is with the Department of Electrical and Information Engineering, Politecnico di Bari, Italy (e-mail: silvano.vergura@poliba.it). *Corresponding author.*

M. Colaprico and M. F. de Ruvo are with the Spin-off APIS-Apulia Intelligent Systems (e-mails: m.colaprico@spinoffapis.com, mf.deruvo@spinoffapis.com).

F. Marino is with the Department of Electrical and Information Engineering, Politecnico di Bari, Italy and with the Spin-off APIS-Apulia Intelligent Systems (e-mail: f.marino@spinoffapis.com).

numerical and in graphical form, and can be collected in a printable report.

The paper is structured as follows. Section II deals with the implementation issues of the procedures encapsulated in the platform, while its GUI is shown in Section III. Section IV discusses several tests performed on operating PV modules, and Conclusions ends the paper.

## II. IMPLEMENTATION ISSUES

The software platform translates the diagnostic workflow summarized in Fig. 1. The role of each algorithmic step enclosed in the phases *PRE-PROCESSING*, *INPUT*, *PROCESSING*, *POST-PROCESSING*, and *OUTPUT* has been described in [14], thus, in this paper we are going to discuss the implementation issues of the above phases.

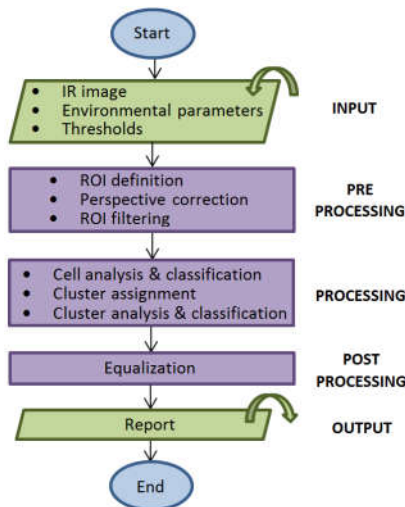


Fig. 1. Phases of the diagnostic workflow.

### A. Input

The Input phase concerns not only the InfraRed (IR) image to be analyzed, but also some environmental parameters and few threshold values, which are needed in order to correctly carry out the diagnostics.

The platform saves these data in a log file and proposes the most recently used as default. In fact, during a maintenance campaign of a PV plant, the analyzed PV devices have often the same structure and characteristic, as well as the IR images may have been acquired under the same environmental conditions. Therefore, iterate the input phase can be avoided, saving time.

### B. Pre-processing

After having loaded the IR image and defined the Region Of Interest (ROI) inscribing the PV module -as later highlighted by the green quadrangle on Fig. 5(a)-, a Preprocessing phase is needed to correct the perspective and, eventually, to reduce the noise.

To correct the perspective is necessary in order to get an “undistorted image” in which all the PV cells are resized to an identical area. To have each cell represented by the same number of IR pixels is mandatory for getting a correct analysis and it is

obtained through an affine transformation, i.e., a function between affine spaces which preserves points, straight lines and planes. An affine transformation does not necessarily preserve angles between lines or distances between points, though it preserves ratios of distances between points lying on a straight line.

In this scenario, the platform corrects the perspective, exploiting the geometrical condition that the four vertexes of the quadrangular ROI should be mapped as vertexes of a rectangle onto the destination (undistorted) space.

In case a noise reduction is needed, as described in Part I [14], the workflow provides three possible filtering strategies based either on a median filter, or on a Gaussian filter, or on a cascade of them. These ones have been implemented employing the C++ methods `medianBlur` and `GaussianBlur`.

### C. Processing

The Processing phase encloses the algorithmic steps which are “strictly” diagnostic, and are (see [14]):

- *Cell analysis*, which investigates the health of each PV cell, through its thermal state, as if this one was not connected to other cells;
- *Cell classification*, in which cells having uniform temperature are studied by comparing the mean temperatures of the cells with the expected temperature determined basing both on the Nominal Operative Cell Temperature (NOCT), and on the environmental conditions, such as irradiance level and air temperature;
- *Cluster assignment*, in which cells having mean temperatures enclosed in a given range are grouped in families called *clusters*;
- *Cluster analysis*, which analyzes each cluster basing on the number of enclosed cells, the position inside the PV module, the mean value of the cluster temperature;
- *Cluster classification* where the clusters are sorted from the *no-problem* ones to the *most critical* one, on the basis of the power loss.

These steps have been implemented by means of a C++ code, in which each PV cell and PV module are represented as “objects” of the *ad hoc* defined classes `PVCell` and `PVModule`, whose main members are recalled in Fig. 2.

An instance of the `PVModule` class encapsulates a 2-D array of `PVCell` objects, organized into `NumberOfRows` rows and `NumberOfColumns` columns. Each cell of such array (say `Cell[i][j]`) is therefore characterized by the variance and the mean computed among all the temperatures inside the cell itself (say respectively, `Cell[i][j].VarianceTemp` and `Cell[i][j].MeanTemp`); these numerical values are initialized by the methods of the class `PVCell`, through the temperature map in the IR image. `Cell[i][j].VarianceTemp` is used to discriminate if `Cell[i][j]` is uniform or not, comparing it with respect to a predefined threshold (say, `UniformityThreshold`); then, in case of uniformity, `Cell[i][j]` is classified through `Cell[i][j].MeanTemp`.

```

class PVCell {
  const float VarianceTemp;
  const float MeanTemp;
  std::stringType;
  int ClusterID; //identifies the cluster assigned to the cell
  // constructors and other methods here not recalled
}
class PVModule {
  std::vector<std::vector <PVCell>> Cell; //2D vector of PVCell
  const int NumberOfRows; // number of rows in Cell[ ][ ]
  const int NumberOfColumns; //number of columns in Cell[ ][ ]
  std::vector<cv::Mat> BinaryImage; //vector of images
  const float MinTemp;
  const float MaxTemp;
  const int NumberOfClusters; //number of clusters in the module
  // constructors and other methods here not recalled
  void CellClassificationAndClustering (); //see Fig. 3
}

```

Fig. 2. PVCell and PVModule classes.

More in detail, the method `CellClassificationAndClustering` (see Fig. 3) assigns a value (among “Non Uniform”, “Normal”, “Light Hot Cell”, “Medium Hot Cell” and “Strong Hot Cell”) to the attribute `Cell[i][j].Type` in function of two thresholds (say, `LightMediumThreshold` and `MediumStrongThreshold`). The same method performs the clustering, too, i.e. it assigns the cells of the module to a certain cluster, simply initializing `Cell[i][j].ClusterID` with the difference between the temperatures `Cell[i][j].MeanTemp` and `MinTemp`, quantized by a factor said `ClusterTemperatureRange`.

```

void PVModule::CellClassificationAndClustering () {
  NumberOfClusters = 1 + (MaxTemp - MinTemp)
  / ClusterTemperatureRange;
  for (i=0; i < NumberOfRows; i++)
    for (j=0; j < NumberOfColumns; j++)
      if (Cell[i][j].VarianceTemp > UniformityThreshold)
        Cell[i][j].Type = "Non Uniform"
      else {
        Cell[i][j].ClusterID = floor ((Cell[i][j].MeanTemp
- MinTemp) / ClusterTemperatureRange;
        if (Cell[i][j].MeanTemp < (NormalityDelta
+ MinTemp))
          Cell[i][j].Type = "Normal"
        else
          if (Cell[i][j].MeanTemp < LightMediumThreshold)
            Cell[i][j].Type = "Light Hot Cell"
          else
            if (Cell[i][j].MeanTemp < MediumStrongThreshold)
              Cell[i][j].Type = "Medium Hot Cell"
            else
              Cell[i][j].Type = "Strong Hot Cell"
      }
}

```

Fig. 3. `CellClassificationAndClustering` method.

Clusters are analyzed mainly basing on blob analysis techniques. Given the PV module `X`, `X.BinaryImage`, a vector of `X.NumberOfClusters` binary images (i.e., having as many elements as the clusters enclosed in the PV module `X`), is created. The binary image `X.BinaryImage[k]` is associated to the cluster `#k` having all its pixels equal to “0”, except those of the cells `X.Cell[i][j]` where `X.Cell[i][j].ClusterID == k`, which are set to “1”.

Therefore, the blob structure of the cluster `#k` is graphically generated applying in `X.BinaryImage[k]` the C++ method `findContours()`, while the number of cells is evaluated using the C++ method `countNonZero()`. The cluster classification is merely performed through the

numeric value of `ClusterID`, which, thanks to the method `CellClassificationAndClustering`, results in an index related to the power loss (higher the index, higher the loss).

#### D. Post-processing

A post processing, basically consisting on an equalization, is applied on the ROIs produced at each step. This allows to assign the whole available 8-bits dynamic only to the temperature range present inside the ROI, i.e., on the PV module. Obviously, this equalization does not modify the temperature values, but only their representation, in order to get a better visualization, as we evidence in the case of study discussed in Section IV.B.

#### E. Output

Once the PV module has been completely analyzed, the platform produces a printable report in PDF format, in which all the input data, and above all the produced results, are collected both in numerical and in graphical form in an *easy-to-interpret* template.

### III. GRAPHICAL USER INTERFACE

Fig. 4 shows a screenshot of the GUI, captured during the “cell analysis” step.

In the top area are visible several buttons. Those on the first line are related each one to a single step of the workflow: once the step *S* is performed, the related button commutates to a dual “back to the *S* step” button, as the case of the first five buttons shown in the screen shot. The long button on the second line, activates instead an *all-in-one* macro, which launches the whole workflow and may be usefully employed in case the environmental parameters and the thresholds are not newly required, being those already saved as default values in the log file (see Section II.A).

The bottom area encloses two windows. The left one is a toolbox structured into four tabs, each one related to the steps: “Load image and setup”, “Filtering”, “Cell analysis” and “Cluster analysis”. These tabs contain spin boxes for inputting values, and buttons related to actions specific of the step, as the analysis launcher and the report generation evidenced in Fig. 4. Moreover, the tabs provide some numerical outputs, that in case of anomalies are displayed in red. Finally, the right side of the GUI encloses dynamical tabs, each one hosting the graphical output of a certain step: these outputs are basically constituted by suitably annotated images, as those shown in the tab of Fig. 4. as well as in the cropped tabs of Figs. 5, 6, and 7.

### IV. RESULTS AND DISCUSSION

In this Section we will present three cases of study.

They are related to a 20 kWp PV plant located on the roof of a building, south-oriented and having a tilt of 40°. The plant has been connected to the grid in 2009, employing PV modules whose datasheet parameters are reported in Table I.

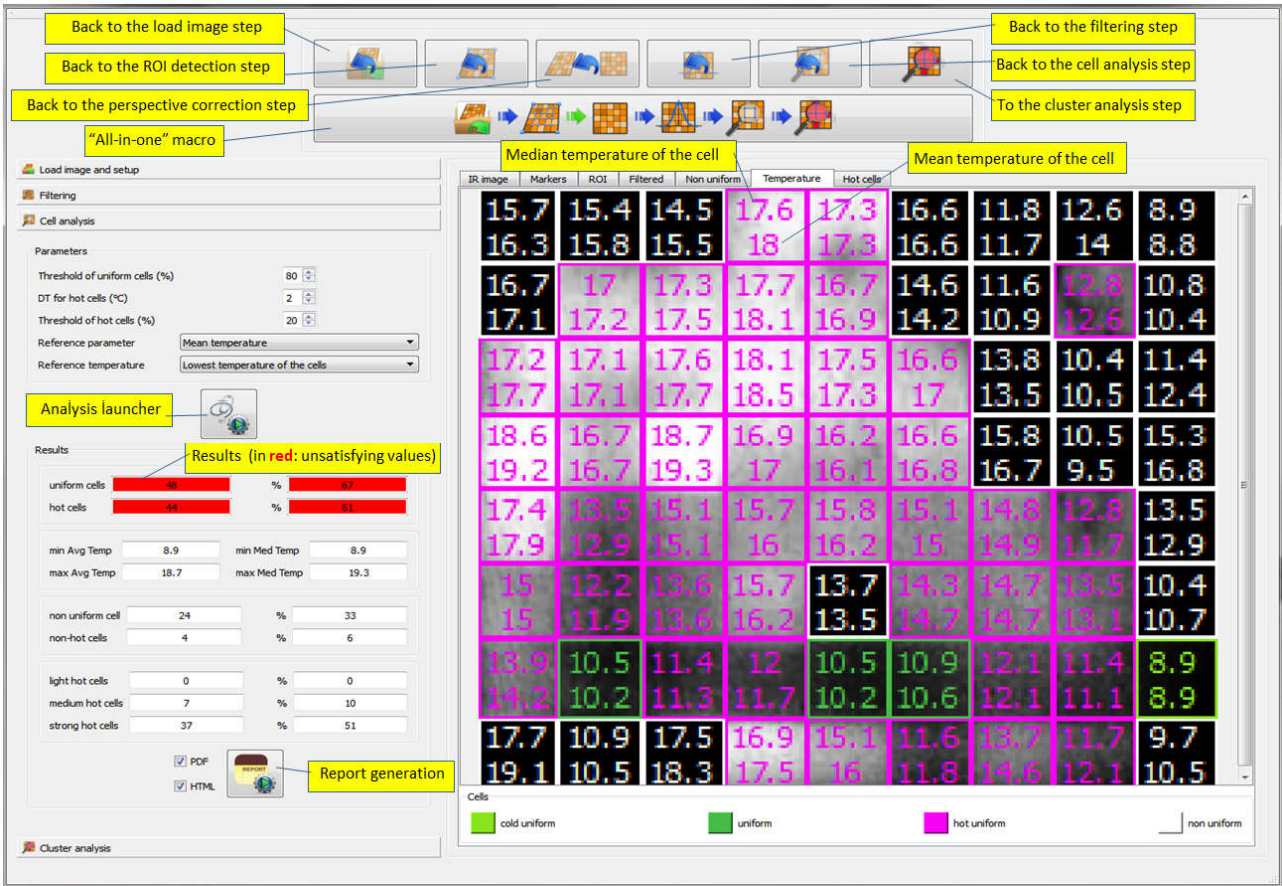


Fig. 4. GUI of the software platform, captured during the *Cell analysis*, with some explicative over imposed call outs.

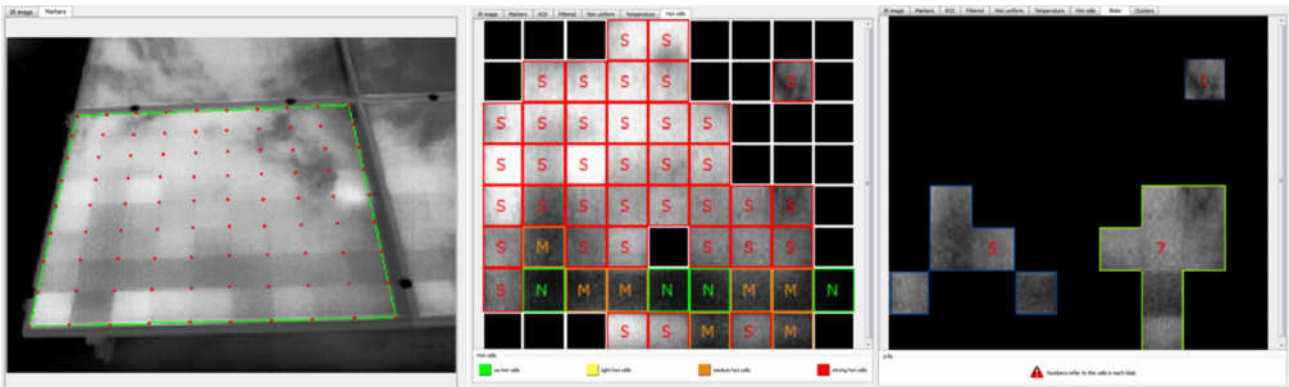


Fig. 5. (a): ROI and grid of the PV cells; (b): non-uniform (black) and normal (green) cells; medium (orange) and strong (red) hot cells; (c): cluster of PV cells, constituted by three blobs, respectively having 1, 5 and 7 cells.

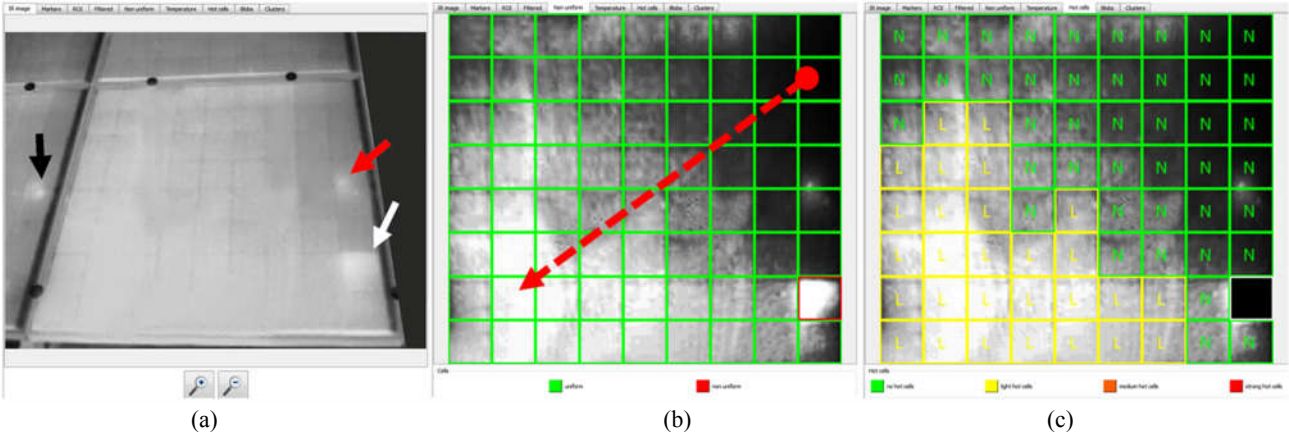


Fig. 6. (a): IR image of an almost completely uniform module; (b): classification uniform vs not uniform cells; (c): normal and hot cells.

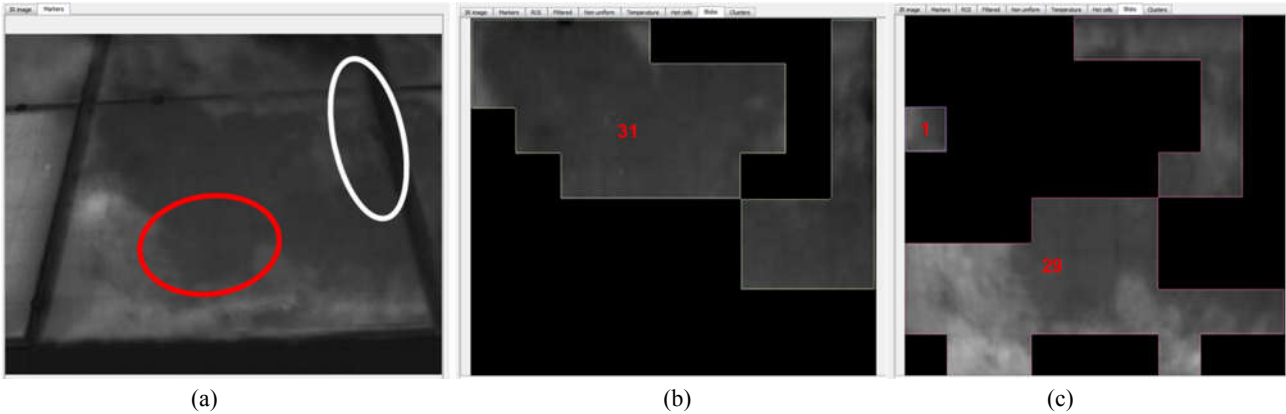


Fig. 7. (a): IR image of a non-uniform module; (b): colder cluster #0; (c): hotter cluster #1.

TABLE I. ELECTRICAL PARAMETERS OF THE INVESTIGATED PV MODULES IN STC (EXCEPT FOR NOCT)

PV module	PhotoWatt
Code	PV1650
Material	Poly-Si
$P_n$ [W]	$175 \pm 3\%$
Voc [V]	43.20
Isc [A]	5.31
Vmpp [V]	34.80
Impp [I]	5.03
NOCT [°C]	$45 \pm 2$

TABLE II. DATASHEET PARAMETERS OF THE EMPLOYED THERMAL-CAMERA (THERMALCAM B4©, BY FLIR©)

Property	Value
Field of view	$23^\circ \times 17^\circ$
Min focus distance	0.3 m
Thermal sensitivity	$0.08^\circ\text{C}$ at $30^\circ\text{C}$
Image frequency	50 Hz non-interlaced
Focus	Manual
Detector type Focal	Focal Plane Array (FPA), uncooled microbolometer 320 x 240 pixels
Spectral range	7.5 to 13 $\mu\text{m}$
Digital zoom	1x, 2x or 4x
Temperature range	$-20^\circ\text{C}$ to $+100^\circ\text{C}$
Operating temperature range	$-15^\circ\text{C}$ to $+50^\circ\text{C}$
Accuracy	$\pm 2^\circ\text{C}$ , $\pm 2\%$
Repeatability	$\pm 1^\circ\text{C}$ , $\pm 1\%$

The employed thermal-camera was the ThermoCAM B4© by FLIR©, whose characteristics are reported in Table II: it can be noted that it is a long-wave thermal-camera (see spectral range). The uncooled detector, having a 320x240 resolution, allows medium-high quality IR images, rigorously measuring and analyzing 76.800 points. It can operate between  $-20^\circ\text{C}$  and  $+100^\circ\text{C}$ , with a thermal sensibility of  $0,08^\circ\text{C}$ , thus making possible the detection of small variations of temperature.

During the acquisitions, the good weather conditions (air temperature equal to  $10^\circ\text{C}$ , solar irradiance of  $650\text{ W/m}^2$ , and relative humidity of 54%) have allowed a correct acquisition of the images, and it has been necessary to set (with particular accuracy) several

specific reference parameters which influence the results. Emissivity has been set to 0.85 (it is related to the material and thickness of the solar glass, and typically ranges from 0.85 to 0.90), while the reflected temperature has been changed during the acquisitions, being dependent on the mutual position of the thermal-camera and the target.

#### A. A defected module

The first case considers the defected PV module of Fig. 5(a), characterized by hot and cold cells, accidentally distributed. The figure shows also the green ROI and the red grid of the cells. Fig. 5(b) puts in evidence the non-uniform cells (black), the uniform well-working cells (green “N”), the medium hot cells (orange “M”), and the strong hot cells (red “S”), as determined by the processing phase.

The platform has pointed out several criticalities that were not perceptible in the source IR image. Firstly, there are 37 strong hot cells, which were masked by the luminance of the strongest one in Fig. 5(b). Secondly, there are 24 non-uniform cells, and many of them are not evident in the IR image. In addition, Fig. 5(b) reveals also 7 *medium* hot spots.

Finally, we report Fig. 5(c), which shows one of the clusters of the PV module: it encloses three blobs, containing 1, 5 and 7 cells, evidencing that the platform allows to group PV cells with the same thermal behavior, even if they are not connected among themselves.

#### B. An almost completely uniform module

The second case concerns a PV module visibly characterized by only one very critical cell, pointed by the white arrow in Fig. 6(a). This circumstance is confirmed by the graphical output of Fig. 6(b), which evidences it in red, as the unique non-uniform cell. Nevertheless, in Fig. 6(c) the cell analysis, after having masked in black that non-uniform cell, highlights also several light hot cells, which were not noticeable by a subjective observation of the input IR image of Fig. 6(a).

Note that the spot indicated by the red arrow in Fig. 6(a) is not a defect, but an over temperature due to the junction box on the rear of the PV module (in fact, the same phenomenon appears replicated in the module on

the left, as evidenced by the black arrow). This hypothesis can be confirmed during the acquisition: in fact, an insufficient insulation between the junction box and the module is revealed as a *systematic* hot spot occurring at the same position in all the modules.

Finally, Fig. 6(b) explicates also the effects of the post processing: in fact in it, thanks to the equalization, the temperature gradient (remarked by the dotted red arrow) appears much more evident than in the input IR image of Fig. 6(a).

### C. A dis-homogeneous module

A third case of study is related to the PV module of Fig. 7(a), visibly characterized by two macro-areas, none of them exactly matching a group of cells. We remark this case in order to focus the attention on the clusters evidenced by the platform:

- a “subjective analysis” might assume that the cells circled by the red curve in Fig 7(a) belong to the colder cluster #0 in Fig. 7(b), whereas the objectivity of the platform has assigned them to the hotter cluster #1;
- in the same way, the cells evidenced by the white ellipse in the Fig. 7(a) might seem belonging to the hotter cluster #1 in Fig. 7(c), instead they have been assigned to the colder cluster #0.

This example evidences that the quantitative analysis, allowed by the platform, assures an aggregation exempt from those subjective errors typical of a qualitative analysis.

## V. CONCLUSIONS

This Part II has presented a software platform which implements the innovative diagnostic workflow to process the IR images of PV modules, that was introduced in Part I [14]. The platform automatically performs all the time-consuming recommended steps, and generates an immediate and detailed report, enclosing numeric and graphic results which are focused both on the cell level and on the cluster level. Moreover, since it provides information on the health state of the PV module, if periodically used, it allows a tracking of its ageing trend, too.

Differently from available commercial software products, which limit the analysis at the PV module level, our platform allows monitoring each single PV cell, thus representing a very important improvement for anyone interested in investigating the reasons of the power loss, and not simply its amount.

In the paper, some cases of study have been also discussed with the aim of highlighting several features of the platform: they put in evidence critical situations that manual analyses of the IR images cannot reveal.

Nowadays, the proposed platform has been implemented in a cloud application [16], in order to provide the users with updated versions, as new features will be added to the workflow.

## REFERENCES

- [1] O. Breitenstein, JP Rakotoniaina, M. H. Al Rifai, and M. Werner, “Shunt type in crystalline solar cells,” *Progress in photovoltaics research and application*, 12, pp. 529-538, 2004.
- [2] J.P. Rakotoniaina, S. Neve, M. Werner, and O. Breitenstein, “Material induced shunts in multicrystalline silicon solar cells,” *Proc. of the Conf. on PV in Europe*, Rome, pp. 24-27, 2002.
- [3] S. Armstrong, and W.G. Hurley, “A thermal model for photovoltaic panels under varying atmospheric conditions,” *Applied Thermal Engineering*, Vol. 30, pp. 1488-1495, 2010.
- [4] S. Vergura, A. Massi Pavan, “On the photovoltaic explicit empirical model: operations along the current-voltage curve”, *IEEE-ICCEP 2015 Int. Conf. on Clean Electrical Power*, Taormina, Italy, June 16–18, 2015.
- [5] S. Vergura, “A Complete and Simplified Datasheet-based Model of PV Cells in Variable Environmental Conditions for Circuit Simulation, *Energies*, 9, no. 5: 326, 2016.
- [6] E. Skoplaki, and J.A. Palyvos, “On the temperature dependence of photovoltaic module electrical performance: A review of efficiency/power correlations,” *Solar Energy*, v. 83, pp. 614–624, 2009.
- [7] J.A. Tsanakasa, D. Chrysostomou, P. N. Botsaris, and A. Gasteratos, “Fault diagnosis of photovoltaic modules through image processing and Canny edge detection on field thermographic measurements,” *Intern. Journal of Sustainable Energy*, pp. 1-22, 2013.
- [8] S. Johnston, H. Guthrey, F. Yan, K. Zaunbrecher, M. Al-Jassim, P. Rakotoniaina, and M. Kaes, “Correlating Multicrystalline Silicon Defect Types Using Photoluminescence, Defect-band Emission, and Lock-in Thermography Imaging Techniques”, *IEEE Journal of Photovoltaics*, Vol. 4, Issue 1, pp. 348-354, 2014.
- [9] M. Peloso, L. Meng and C.S. Bhatia, “Combined thermography and luminescence imaging to characterize the spatial performance of multi-crystalline Si wafer solar cells”, *IEEE Journal of Photovoltaics*, Vol. 5, Issue 1, pp. 102-111, 2015.
- [10] O. Breitenstein, J. Bauer, K. Bothe, D. Hinken, J. Müller, W. Kwapiel, M.C. Schubert, W. Warta, “Can luminescence imaging replace lock-in thermography on solar cells?”, *IEEE Journal of Photovoltaics*, Vol. 1, Issue 2, pp. 159-167, 2011.
- [11] Y. Hu, W. Cao, J. Ma, S.J. Finney, and D. Li, “Identifying PV Module Mismatch Faults by a Thermography-Based Temperature Distribution Analysis,” *IEEE Transactions on Device and Materials Reliability*, Vol. 14, No. 4, December 2014,
- [12] A. Dolara, S. Leva, G. Manzolini, and E. Ogliaari, “Investigation on Performance Decay on Photovoltaic Modules: Snail Trails and Cell Microcracks,” *IEEE Journal of Photovoltaics*, Vol. 4, n. 5, pp 1204-1211, September 2014.
- [13] Y. Hu, W. Cao, J. Wu, B. Ji, and D. Holliday, “Thermography-Based Virtual MPPT Scheme for Improving PV Energy Efficiency Under Partial Shading Conditions,” *IEEE Transactions on Power Electronics*, Vol. 29, no. 11, pp. 5667-5672, 2014.
- [14] S. Vergura, F. Marino, “A Quantitative and Computer Aided Thermography-based Diagnostics for PV Devices: Part I – Framework”, submitted to *IEEE Journal of Photovoltaics*.
- [15] <http://opencv.org>
- [16] <http://www.diss.cloud>